

1 **Source attribution and process analysis for atmospheric mercury in**  
2 **East China simulated by CMAQ-Hg**

3  
4 Jialei Zhu<sup>1</sup>, Tijian Wang<sup>1</sup>, Johannes Bieser<sup>2,3</sup>, Volker Matthias<sup>2</sup>

5 1. School of Atmospheric Sciences, Nanjing University, Nanjing 210093, China

6 2. Institute of Coastal Research, Helmholtz-Zentrum Geesthacht, Max-Planck-Str. 1,  
7 21502, Geesthacht, Germany

8 3. National aeronautics and space research center (DRL), Oberpfaffenhofen, 82234,  
9 Weßling, Germany

10 Correspondence to: Tijian Wang (tjwang@nju.edu.cn)

11  
12 **Abstract**

13 The contribution from different emission sources and atmospheric processes to  
14 gaseous elemental mercury (GEM), gaseous oxidized mercury (GOM), particulate  
15 bound mercury (PBM) and mercury deposition in East China were quantified using  
16 the Community Multi-scale Air Quality (CMAQ-Hg) modeling system run with a  
17 nested domain. Natural source (NAT) and six categories of anthropogenic mercury  
18 sources (ANTH) including cement production (CEM), domestic life (DOM),  
19 industrial boilers (IND), metal production (MET), coal-fired power plants (PP) and  
20 traffic (TRA) were considered for source apportionment. NAT was responsible for  
21 36.6% of annual averaged GEM concentration which was regarded as the most  
22 important source for GEM in spite of obvious seasonal variation. Among ANTH, the  
23 influence of MET and PP on GEM were most evident especially in winter. ANTH  
24 dominated the variations of GOM and PBM concentration with a contribution of  
25 86.7% and 79.1% respectively. Among ANTH, IND was the largest contributor for  
26 GOM (57.5%) and PBM (34.4%) so that most mercury deposition came from IND.  
27 The effect of mercury emitted from out of China was indicated by >30% contribution

28 to GEM concentration and wet deposition. The contribution from nine processes  
29 consisting of emissions (EMIS), gas-phase chemical production/loss (CHEM),  
30 horizontal advection (HADV), vertical advection (ZADV), horizontal advection  
31 (HDIF), vertical diffusion (VDIF), dry deposition (DDEP), cloud processes (CLDS)  
32 and aerosol processes (AERO) were calculated for processes analysis with their  
33 comparison in urban and non-urban regions of Yangtze River Delta (YRD). EMIS and  
34 VDIF affected surface GEM and PBM concentration most and tended to compensate  
35 each other all the time in both urban and non-urban areas. However, DDEP was the  
36 most important removal process for GOM with  $7.3 \text{ ng m}^{-3}$  and  $2.9 \text{ ng m}^{-3}$  reduced in  
37 the surface of urban and non-urban areas respectively in a whole day. Diurnal profile  
38 variation of processes revealed the transportation of GOM from urban area to non-  
39 urban area and the importance of CHEM/AERO in higher altitudes which caused  
40 diffusion of GOM downwards to non-urban area partly. Most of the anthropogenic  
41 mercury transported and diffused away from urban area by HADV and VDIF and  
42 increase mercury concentration in non-urban areas by HADV. Natural emissions only  
43 influenced CHEM and AERO more significantly than anthropogenic. Local emission  
44 in the YRD contributed 8.5% more to GEM and ~30% more to GOM and PBM in  
45 urban areas compared to non-urban areas.

46

## 47 **1 Introduction**

48 Mercury (Hg) pollution in the atmosphere attracts increasing concern globally in  
49 view of its neurotoxicity and bioaccumulation in along the food chain posing risks to  
50 human health (Schroeder and Munthe, 1998; Rolffhus et al., 2003). Atmospheric  
51 mercury is divided into three species according to various physical and chemical  
52 properties: gaseous elemental mercury (GEM), gaseous oxidized mercury (GOM) and  
53 particulate bound mercury (PBM). GEM is the predominant form (>95%) in  
54 atmosphere; it is very stable and well-mixed hemispherically with a long lifetime of

55 0.5~2 years (Selin et al., 2007). In contrast, GOM and PBM will deposit more rapidly  
56 downwind of their emission sources via wet or dry deposition since GOM and PBM  
57 have significantly higher reactivity, deposition velocities, and water solubility (Lin  
58 and Pehkonen, 1999; Lindberg et al., 2002; Keeler et al., 2005). Accordingly, mercury  
59 is a multi-scale pollutant able to be transported at local, regional and long scale  
60 distances from the sources and mercury emission speciation has a great impact on  
61 processes and spatial distribution of mercury in the atmosphere (Bieser et al., 2014;  
62 Quan et al., 2009; Voudouri and Kallos, 2007; Pai et al., 1999).

63 Mercury is released into the atmosphere from both natural processes and  
64 anthropogenic activities. Natural processes such as evasion from soils, water bodies  
65 and vegetation just emit GEM with evident seasonal variation (Shetty et al., 2008).  
66 The natural sources will also include re-emission of anthropogenic mercury deposited  
67 into the environment previously (Gbor et al., 2006). Mercury emissions from  
68 anthropogenic sources are mainly from coal combustion, non-ferrous smelters, waste  
69 incineration and mining (Streets, et al., 2009). Anthropogenic mercury emissions in  
70 Asia are the highest in the world, accounting for about half of the global total (Pacyna  
71 et al. 2010). Especially, China is considered as one of the largest and growing source  
72 regions due to its rapid economic and industrial growth along with a coal-dominated  
73 energy structure (Wu et al., 2006; Wang et al., 2014). Particularly high emissions of  
74 mercury in China result in more elevated mercury concentration and larger mercury  
75 deposition than background levels in the world even in remote areas such as the Mt.  
76 Gongga area (Fu et al., 2008) and Mt. Changbai (Wan et al., 2009). Much more  
77 serious atmospheric mercury pollution was detected in Chinese urban sites where total  
78 gaseous mercury (TGM) concentrations were a factor of 3~5 higher than those  
79 observed in rural areas (Zhu et al., 2012; Chen et al., 2013; Feng et al., 2004, Zhang et  
80 al., 2013). Therefore, improving the understanding of the source-receptor  
81 relationships for mercury and providing valuable information on mercury transport,

82 deposition and chemistry within China are urgently needed. Detailed quantitative  
83 assessments of the contribution of mercury sources help to determine effective  
84 mercury emission control strategies.

85 Previous publications provided contribution estimates from selected emission  
86 sources mostly in the United States (Seigneur et al., 2004; Selin and Jacob, 2008; Lin  
87 et al., 2012) and the Great Lakes (Cohen et al., 2004; Holloway et al., 2012) using  
88 global and regional chemical transport models. Many studies for Asia focus on the  
89 mercury mass outflow caused by the total emission in Asia and its contribution to long  
90 range transport (Pan et al., 2010; Lin et al., 2010). Limited source apportionment of  
91 mercury pollution in China has been studied by Wang et al. (2014) distinguishing four  
92 emission sectors using a global model (GEOS-Chem) in coarse spatial resolution. In  
93 addition, few studies focus on diagnostic and process analysis for atmospheric  
94 mercury pollution formation and identification of the dominant atmospheric processes  
95 for mercury. The mercury version of US EPA's Community Multi-scale Air Quality  
96 (CMAQ-Hg) modeling system (Bullock and Brehme, 2002) was widely used to  
97 simulate regional atmospheric mercury pollution. Process analysis (PA) embedded in  
98 CMAQ can be applied to investigate the relative contribution of the individual  
99 processes on simulated concentration. The performance of CMAQ-Hg model in  
100 simulating mercury has been evaluated against mercury concentration and deposition  
101 measured on surface mostly in US (Holloway et al., 2012; Bullock et al., 2008, 2009;  
102 Gbor et al., 2006, 2007).

103 In this paper, the temporal and spatial distribution of atmospheric mercury and its  
104 deposition in 2011 were simulated on a nested domain over East China with grid  
105 resolution of 27x27 km<sup>2</sup> and parent grid resolution of 81x81 km<sup>2</sup> using CMAQ-Hg.  
106 The model results were compared to available monitoring data. Seasonal  
107 contributions of all types of mercury emission sources, including natural emissions,  
108 cement plants, domestic coal burning, industrial boilers, metal productions, power

109 plants and traffic emissions, to atmospheric mercury concentration and deposition  
110 were quantified. The process analysis for atmospheric mercury concentration was  
111 used for select urban and non-urban areas. The influence of physical and chemical  
112 processes on mercury concentration was examined. This study provides a detailed  
113 model study on source apportionment and process analysis of atmospheric mercury in  
114 East China.

115

## 116 **2 Methods**

### 117 **2.1 Model descriptions**

118 The model used in this study was based on CMAQ v4.6 which has been modified  
119 by Bullock and Brehme (2002) and Gbor et al. (2006) to include chemistry, transport  
120 and deposition of GEM, GOM and PBM. The model was configured to use the  
121 Carbon Bond 5 (CB05) gaseous phase chemistry mechanism (Sarvar et al., 2008) with  
122 Euler Backward Iterative (EBI) solver and the AERO4 aerosol mechanism  
123 (Binkowski and Roselle, 2002). The CB05 mechanism used here included mercury  
124 gaseous reactions with ozone, OH, H<sub>2</sub>O<sub>2</sub> and Cl<sub>2</sub> as described by Lin and Tao (2003).  
125 The meteorological fields used in CMAQ-Hg were provided by the Weather Research  
126 and Forecasting (WRF v3.2) Model. Meteorology-Chemistry Interface Processor  
127 (MCIP v3.6) processed the WRF outputs to the CMAQ-Hg model-ready format and  
128 dry deposition velocities of GEM and GOM were calculated. The process analysis  
129 (PA) technique is an advanced diagnostic method implemented in CMAQ. It provides  
130 hourly integrated process rates to quantify the changes in concentration from each of  
131 the scientific processes in the mass conservation equations being solved for each  
132 mercury species. During this simulation, the contributions from following physical  
133 and chemical processes were calculated: emissions of mercury species (EMIS), net  
134 gas-phase chemical production/loss (CHEM), horizontal advection (HADV), vertical  
135 advection (ZADV), horizontal diffusion (HDIF), vertical diffusion (VDIF), dry

136 deposition (DDEP), cloud processes (CLDS, including cloud attenuation of photolytic  
137 rates, convective and non-convective mixing and scavenging by clouds, aqueous-  
138 phase chemistry, and wet deposition), aerosol processes (AERO, including  
139 thermodynamic equilibrium and dynamics such as homogeneous nucleation,  
140 condensation/evaporation, and coagulation) (Liu and Zhang, 2013).

141

## 142 **2.2 Emission inventory**

143 Both anthropogenic and natural emission inventories of mercury were employed  
144 in our simulation with CMAQ-Hg. Emissions from natural sources (NAT) including  
145 vegetation, soil surface and water bodies were based on the estimates by Shetty et al.  
146 (2008). GEM is the only species emitted from natural sources. Secondary emissions  
147 that resulted from deposited mercury transformed to GEM and re-emitted to the  
148 atmosphere from soil and water were also considered. Anthropogenic mercury  
149 emissions in China were prepared following the approaches of Wang et al. (2014),  
150 which were updated to 2007 (Figure 1a). The inventory data were not consistent with  
151 our modeling period, but represented the most updated data at the time when this  
152 study was conducted. The monthly variation of anthropogenic sources was based on  
153 the monthly energy consumption and product yields published in the Chinese  
154 yearbook of provincial diversity. The ratios of three mercury species released were  
155 varied according to many factors like coal produced in different provinces, mercury  
156 content in coal consumed, different boiler types and removal efficiencies and different  
157 combinations of atmosphere pollution control devices (Wang et al., 2014). The total  
158 anthropogenic mercury sources (ANTH) in China were classified into six categories  
159 for source apportionment: (1) emission from cement production (CEM), (2) emission  
160 from domestic life (DOM), which includes waste incineration, domestic coal burning  
161 and application of battery and fluorescent lighting, (3) emission from industrial  
162 boilers (IND) including boilers used for collective heating in North China during

163 winter, (4) emission from metal production (MET) including zinc smelters, lead  
164 smelters, copper smelters, iron production, mercury production and gold production,  
165 (5) emissions from coal-fired power plants (PP), which were all treated as large point  
166 sources in our simulation, (6) emission from traffic (TRA). Table 1 summarizes the  
167 emission inventory for China (land area in the outermost model domain) in 2007. The  
168 annual total anthropogenic emissions amount to  $638 \text{ Mg year}^{-1}$  which was comparable  
169 to natural emissions of  $551 \text{ Mg year}^{-1}$ . The average speciation of anthropogenic  
170 emissions is as follows: (GEM 49.5%, GOM 38.4%, and PBM 12.1%).

171

### 172 **2.3 Model domain and scenarios**

173 The modeling period covers one year from 20 December 2010 to 31 December  
174 2011 including an 11 days spin-up period. Two nested domains were used for CMAQ-  
175 Hg model. The first domain (D01, Figure 1a) covers most of China and some other  
176 parts of Asia with  $85 \times 72$  horizontal grid cells at a spatial resolution of  $81 \text{ km} \times 81 \text{ km}$ .  
177 The initial and boundary condition for D01 modeling were extracted from GEOS-  
178 Chem global simulation results. The nested domain (D02, Figure 1b) was defined  
179 over East China area which is the focus of this study. D02 contains  $82 \times 67$  horizontal  
180 grids with a spatial resolution of  $27 \text{ km} \times 27 \text{ km}$ . There were 27 vertical layers with a  
181 top layer pressure of 100 hPa for both domains. The Yangtze River Delta (YRD)  
182 (Figure 1c) is one of the most industrialized and urbanized regions in East China and  
183 mercury pollution has become a problem of increasing concern, thus the YRD was  
184 chosen for process analysis. Figure 1c showed the land use in the YRD which was  
185 divided into three categories of urban, non-urban and water body. A comparison was  
186 made of characteristics of processes influencing atmospheric mercury species in urban  
187 and non-urban.

188 Nine emission scenarios in China were considered to understand the relative  
189 importance of different emission sources to atmospheric mercury concentration and

190 deposition. The base case (BASE) was run with both natural and all anthropogenic  
191 sources mentioned above. Seven sensitivity studies (C1~C7) were designed with one  
192 of seven source sectors (i.e. NAT, CEM, DOM, IND, MET, PP and TRA) excluded in  
193 each study. In addition, the boundary conditions (BC) were set to zero (C8).  
194 Subtracting the results of C1~C8 from the BASE case yields an estimate of mercury  
195 associated with these mercury sources.

196

### 197 **3 Results and discussion**

#### 198 **3.1 Model validation**

199 The spatial distribution of annual average concentration and annual total  
200 deposition of GEM, GOM and PBM simulated in BASE are shown in Figure 2. The  
201 predicted annual average concentration of GEM, GOM and PBM were in the ranges  
202 of 1.8~8.4 ng m<sup>-3</sup>, 0.015~1.5 ng m<sup>-3</sup> and 0.017~1.3 ng m<sup>-3</sup>. On average, GEM  
203 constituted 92.8% of the total atmospheric mercury with the contribution going down  
204 to a minimum of 58.6% near large anthropogenic sources (Figure 2a). The  
205 concentration of GOM and PBM was typically greater at locations of large cities due  
206 to the larger anthropogenic emission there and decreased rapidly away from source  
207 locations because of their relatively shorter atmospheric lifetimes (Figure 2b,2c). The  
208 total mercury deposition was 65.3 μg m<sup>-2</sup> year<sup>-1</sup> with 34.3 μg m<sup>-2</sup> year<sup>-1</sup> of total dry  
209 deposition and 31.0 μg m<sup>-2</sup> year<sup>-1</sup> of total wet deposition. The dry deposition of GEM  
210 was 4.26 μg m<sup>-2</sup> year<sup>-1</sup> on average with the larger deposition in the southern part of  
211 D02 due to the larger dry deposition velocity of GEM there (Figure 2d). GOM  
212 contributed 28.2 μg m<sup>-2</sup> year<sup>-1</sup> to total dry deposition with a range of 2.5~428.4 μg m<sup>-2</sup>  
213 year<sup>-1</sup>, which was the dominant fraction of mercury dry deposition. The distribution  
214 of the dry deposition of GOM and PBM resembled the spatial pattern of urban area in  
215 East China as a result of high concentration of GOM and PBM there, especially  
216 showing the elevated deposition in the eastern (i.e. YRD) and northern part of D02



217 (Figure 2e, 2f). The wet deposition was dominated by PBM (56.5%) followed by  
218 GOM (43.4%). The distribution of wet deposition was affected by the spatial pattern  
219 of concentration and precipitation (Figure 2h, 2i). The wet deposition of GEM was  
220 negligible due to its low solubility in water (Figure 2g).

221 The results from the base case were compared to observations to give a  
222 preliminary evaluation of model performance. As long-term mercury measurements in  
223 East China are very limited, all available measurement results (listed in Zhu et al.,  
224 2012; 2014) in East China were used to assess model skill, of which TGM  
225 concentrations were obtained in nine sites, PBM concentrations were obtained in five  
226 sites and wet deposition was only observed in Nanjing. The locations of these sites are  
227 given in Figure 1b. Although the analysis in the following sections uses the model  
228 results for 2011, the same timeframe with observations reported was simulated for  
229 model validation. Figure 3 shows the comparison between averaged measurements  
230 and CMAQ results during homologous months. Most sites such as Chengshantou (Ci  
231 et al., 2011a), Ningbo (Nguyen et al., 2011), Guangzhou (Chen et al., 2013), Jiaying  
232 (Wang et al., 2007), Mt. Dinghu (Chen et al., 2013), Chongming (Dou et al., 2013),  
233 Nanjing (Zhu et al., 2012) and Yellow Sea (Ci et al., 2011b), the simulated TGM is  
234 quite consistent with observations with relative bias of 4%~28% (Figure 3a). In  
235 comparison, modeled TGM concentrations in Pudong were ~51% overestimated. The  
236 site in Pudong (Friedli et al., 2011) was located at a coastal urban area with less than  
237 one month measurement data. The short duration of this measurement and unexpected  
238 complex emission and meteorological condition may be responsible for the larger  
239 bias. The correlation coefficient between averaged observed and simulated TGM  
240 concentration in all sites was 0.85. The model can reproduce the averaged TGM  
241 concentration in most areas of East China, but the model results have a smaller  
242 variability especially in urban sites like Nanjing where the standard deviation of  
243 simulation result was  $4.86 \text{ ng m}^{-3}$  lower than that observed. This is expected to be the

244 incapability of the model to capture emission plumes and predict the transient peaks  
245 observed in urban sites because of the 27 km grid cell resolution and assumption of  
246 instantaneous emission dilution in grid cells (Pongprueksa et al., 2008). As seen in  
247 Figure 3b, the model results were also comparable to PBM concentration observed in  
248 Nanjing (Zhu et al., 2014), Shanghai (Xiu et al., 2009) and Hefei (Wang, 2010). PBM  
249 concentration in Nanjing was underestimated by 60% which may be because the  
250 location of the observation site in Nanjing is in the central urban area with much  
251 higher particle concentration compared to the averaged concentration in the  
252 simulation grid cell. The scarcity of mercury deposition measurement in East China  
253 limited the evaluation of model performance for mercury deposition. Our model result  
254 agrees reasonably well with mercury wet deposition measurement result in Nanjing  
255 site during 9 months in 2011 (Zhu et al., 2014) with  $6.3\mu\text{g m}^{-2}$  underestimated which  
256 was caused by 232.8mm (21.8% to total) less precipitation and less PBM  
257 concentration in urban area predicted. Overall, our simulation did well in reflecting  
258 the levels and deposition of atmospheric mercury in East China and it is suitable for  
259 further analysis of source apportionment.

260

## 261 **3.2 Source apportionment**

### 262 **3.2.1 Natural Sources (NAT)**

263 Figure 4 and Figure 5 summarize annual and seasonal relative contribution of  
264 different source sectors to atmospheric mercury concentration and deposition in East  
265 China (land area in D02). Annual total mercury emissions from natural sources were  
266 close to those from anthropogenic sources. Because all natural emissions are in the  
267 form of GEM, this sector is responsible for 63.6% of the total annual GEM emission  
268 in China. The result was that natural sources are the largest contributor to atmospheric  
269 GEM concentration (36.6% in annual average). Due to significant seasonal variation  
270 of GEM emission from NAT, the contribution from NAT to GEM varied between

271 52.2% in summer and 15.0% in winter. NAT was much more important for GEM  
272 concentration in summer with a factor of 3.3 to the contribution from ANTH (15.9%).  
273 Though GEM was not the key species for mercury deposition, NAT was still an  
274 important contribution to wet and dry deposition in summer with 28.5% and 24.3%  
275 respectively. That was because of higher emission quantity of NAT and the increased  
276 photochemical activities in summer that led to a greater degree of GEM oxidation to  
277 GOM and transformation to PBM, which contributed 15.7% of GOM and 24.2% of  
278 PBM in summer. In contrast, NAT contributes little to GOM concentration (0.2%),  
279 PBM concentration (0.3%) and deposition (2.4% to wet deposition and 1.7% to dry  
280 deposition) in winter. Therefore, during winter, ANTH had a much larger impact on  
281 atmospheric mercury concentration and deposition. The effect from NAT was  
282 decreasing from south to north in mainland of D02, correlating with air temperature.  
283 There was no obvious difference between the quantities contributed from NAT to  
284 urban and rural areas but the relative contribution to urban areas was lower due to  
285 higher emissions and thus concentration and deposition in urban areas.

286

### 287 **3.2.2 Cement production (CEM)**

288 In 2011, anthropogenic sources emitted 638 Mg of mercury which was a little  
289 more than that from natural sources (551 Mg year<sup>-1</sup>). However, unlike natural sources,  
290 mercury from ANTH includes GEM, GOM and PBM. The quantity and speciation of  
291 mercury released from six anthropogenic source categories were quite different. This  
292 leads to different impacts on the spatial and temporal distribution of atmospheric  
293 mercury concentration and deposition.

294 Total mercury emission from CEM is responsible for 13.5% of the total  
295 anthropogenic emissions and ~80% of the mercury from CEM was in the form of  
296 GEM. CEM contributed 6.6% to the total annual GEM concentration which was  
297 23.9% of the total contribution from all anthropogenic sources. The impact on GOM

298 and PBM concentration from CEM was much lower than that of most other  
299 anthropogenic sources. As GEM had little impact on mercury deposition, CEM  
300 changed wet and dry deposition by only 4.0% and 5.1% respectively. The seasonal  
301 variation of the contribution from CEM was negligible because of the production of  
302 cement was relatively constant over the whole year. CEM affected the GEM  
303 concentration in the eastern coastal area most evidently with up to 20% because of the  
304 large emissions from cement plants in the Shandong, Jiangsu and Zhejiang provinces  
305 which are responsible for ~26% of the total emissions from CEM in China.

306

### 307 **3.2.3 Industrial boilers (IND)**

308 Emissions of total mercury from IND made up 32.9% of all anthropogenic  
309 emissions in China. Thus, it is the most important anthropogenic source. Moreover,  
310 70.8% of the total mercury emitted from IND was GOM which makes up 60.8% of  
311 the total GOM emissions in China. Moreover, IND was also the largest source of  
312 PBM in China. Owing to the large quantity of GOM and PBM which can deposit near  
313 the emission sources through dry and wet deposition, IND makes the largest  
314 contribution to mercury deposition with 22.3% and 43.6% to annual wet and dry  
315 deposition corresponding to 57.5% and 34.4% contribution to annual averaged GOM  
316 and PBM concentration. Especially in winter, IND dominated the GOM concentration  
317 and mercury dry deposition with the contribution reaching 73.3% and 63.9%  
318 respectively as a result of large-scale collective heating in northern China. The  
319 measurement by Zhang et al. (2013) also indicated the boilers play an important role  
320 in the elevation mercury concentration in winter of rural Beijing.

321

### 322 **3.2.4 Power plants (PP)**

323 Emissions from PP were another important sector and they were treated as point  
324 sources in the model. GEM and GOM are the main species emitted from PP with a

325 percentage of 68.1% and 30.8% and, in contrast, with only 1.1% of PBM. PP was the  
326 smallest contributor (2.5%) to PBM. However, PP was the second largest contributor  
327 to GEM and GOM concentration (7.1% and 9.6% respectively) among all  
328 anthropogenic sources, although its contribution to GOM concentration was much  
329 lower than the largest GOM sources of IND. Emissions from PP were responsible for  
330 5.5% and 9.8% of wet and dry deposition which resulted from significant impact on  
331 GOM concentration. There were many larger coal-fired power plants with capacities  
332 larger than 1000 MW concentrating in the YRD. Because of this, obviously higher  
333 emission intensity from PP led to a much higher influence to atmospheric mercury  
334 pollution in the YRD with an annual averaged contribution to TGM of up to  $1 \text{ ng m}^{-3}$   
335 (>20%).

336

### 337 **3.2.5 Metal production (MET)**

338 MET was the largest anthropogenic source of GEM accounting for 31.8% of the  
339 anthropogenically emitted GEM. As this sector includes manufacturers and smelters  
340 of various iron and non-iron metals, the content of mercury from MET varied greatly  
341 depending on production process and the mercury content in raw materials. The  
342 speciation factors ranged from 65% to 89% for GEM, 6% to 30% for GOM, and 0%  
343 to 17% for PBM. Overall, MET contributed 8.4%, 8.2% and 5.0% to GEM, GOM and  
344 PBM concentration and was responsible for 4.7% and 7.2% of the annual wet and dry  
345 deposition in East China respectively. Although MET was distributed widely in East  
346 China, the effects of emissions from MET were greatest in Shaanxi Province due to  
347 high mercury concentrations in zinc ore and some small scale plants with poor  
348 mercury control devices (Wu et al., 2012).

349

### 350 **3.2.6 Domestic life (DOM) and traffic emission (TRA)**

351 Emissions from DOM (6.3%) and TRA (4.4%) were the small fraction of

352 anthropogenic sources. They both hardly affected GEM concentration with a  
353 contribution of less than 1% and had little influence on GOM concentration (4.4%  
354 from DOM and 1.8% from TRA). However, over 50% of total PBM emission came  
355 from DOM and TRA and they increased the annual averaged PBM concentration by  
356 24.4% and 8.0% respectively. As PBM was the main component in mercury wet  
357 deposition, DOM was the most important anthropogenic contributor (9.1%) to wet  
358 deposition except IND (22.3%). In contrast, DOM and TRA were the two smallest  
359 contributors to mercury dry deposition with the proportion of 4.8% and 1.9% because  
360 GOM was the dominant contributor to mercury dry deposition. The distribution of  
361 emissions from TRA was very heterogeneous with the majority emitted in large cities.  
362 In spite of the lower total emissions from TRA, the impacts on PBM concentration  
363 and deposition were much higher in and around the province capitals and other large  
364 cities by a factor of 2~20 compared to rural areas.

365

### 366 **3.2.7 Long-range transport (BC)**

367 The impacts of boundary conditions (BC) were also significant for mercury  
368 pollution in East China, which indicates the contribution of mercury emission from  
369 other source regions. GEM can be transported far beyond the regions where it is  
370 emitted and it is hardly deposited. Therefore, GEM in the global mercury pool  
371 affected the concentration in China evidently suggested by our simulation result with  
372 up to 34.3% annual averaged GEM concentration from BC. However, BC have little  
373 effect on GOM concentration with a contribution of only 8.6% because of its  
374 relatively short lifetime. The contribution to GEM concentration from BC was largest  
375 in winter while the contribution was least to GOM concentration then because of  
376 relatively weaker emissions of GEM and stronger emission of GOM in China during  
377 winter. BC influenced the annual averaged PBM concentration by 13.3% due to the  
378 low dry deposition velocity of fine size PBM. As PBM was removed mainly by wet

379 deposition, BC contributed 32.3% to annual wet deposition of mercury in China. In  
380 comparison, only 15.4% of annual dry deposition was linked to BC owing to the small  
381 contribution to GOM. Lin et al. (2012) estimated that 89.1% of mercury dry  
382 deposition and 93.2% of mercury wet deposition in contiguous US regions are caused  
383 by global sources, which is much higher than that ratio estimated for East China in  
384 this study. One of the reasons for this is the much higher local anthropogenic emission  
385 of mercury in China. Moreover, the anthropogenic sources out of China were not  
386 defined accurately. The underestimate of emission sources from other countries  
387 would lead to less contribution from BC to East China.

388

### 389 **3.3 Process analysis**

390 Figure 2 depicts the simulated concentration and deposition of mercury species  
391 during 2011 in East China, which indicated that the Yangtze River Delta (YRD) is one  
392 of most polluted areas with high mercury concentration and deposition. Also, the  
393 YRD is one of the most active areas of human activity in China. Therefore, the YRD  
394 area which is shown in Figure 1c was chosen to study the influence of each physical  
395 and chemical process implemented in CMAQ on atmospheric mercury. The area was  
396 divided into urban, non-urban and water body depends on the predominant land use.  
397 The area with urban coefficient of land use more than 10% was defined as urban area  
398 in this study. Comparisons of the contribution of each process to urban and non-urban  
399 mercury concentrations were studied.

400

#### 401 **3.3.1 Controlling processes**

402 The annual averaged diurnal variations of the contribution from nine processes  
403 which included horizontal advection (HADV), vertical advection (ZADV), horizontal  
404 diffusion (HDIF), vertical diffusion (VDIF), emissions (EMIS), dry deposition  
405 (DDEP), cloud physics and scavenging (CLDS) and gas and aerosol phase chemistry

406 (CHEM/AERO) to the concentration of GEM, GOM and PBM in the near-surface  
407 layer (the first layer in model which was about 50m) in urban and non-urban areas of  
408 the YRD are shown in Figure 6. The results indicate that two major processes  
409 dominate surface GEM concentration, namely EMIS and VDIF and their  
410 contributions were comparable in urban and non-urban area (Figure 6a). The  
411 contributions of EMIS and VDIF to the change of GEM concentration were  
412 noticeably temporally variable with much higher values during mid-day. Their  
413 contribution in midnight were >5 times larger than those at night and they tended to  
414 compensate each other all of the time. The effect of EMIS extended gradually in  
415 daytime along with the increase of temperature and solar radiation which led to higher  
416 emission from NAT. Anthropogenic activity and production are more active during  
417 day time which raised the emissions of mercury, especially in urban area. EMIS was  
418 the only processes with a positive contribution to GEM concentration in urban areas  
419 with annual average of  $1.26 \text{ ng m}^{-3} \text{ h}^{-1}$  and other processes all played the opposite  
420 role. However, HADV and ZADV could contribute to both gain and loss of GEM in  
421 non-urban area throughout the day. Advection processes had more significant  
422 influence on surface GEM concentration during the evening and early morning in  
423 both urban and non-urban areas but ZADV had the opposite effect with a positive  
424 influence in non-urban and a negative in urban areas at night possibly because of the  
425 strong heat island circulation. Processes of DDEP and CLDS made small  
426 contributions to the loss of GEM. On average, they reduced the concentration of GEM  
427 by about  $0.8 \text{ ng m}^{-3}$  per day in urban and non-urban areas.

428 Unlike GEM, the contributions from different processes on surface GOM and  
429 PBM concentrations were much lower in non-urban than that in urban areas due to  
430 lower emissions of GOM and PBM in non-urban areas (Figure 6b, 6c). EMIS and  
431 VDIF were also the dominant processes to change surface GOM and PBM  
432 concentrations similar to GEM. However, DDEP and CLDS were two additional



433 dominant processes influencing GOM and PBM because of higher dry deposition  
434 velocity and reactivity of GOM and PBM. Particularly for GOM, DDEP was the most  
435 important removal process with the surface concentration of  $7.3 \text{ ng m}^{-3}$  and  $2.9 \text{ ng m}^{-3}$   
436 reduced in urban and non-urban area respectively in a whole day. Local dry deposition  
437 of GOM was about 48% of local emissions in urban areas while that in non-urban  
438 areas was 42% larger than local emissions which was affected by the emissions from  
439 nearby urban areas. In addition, VDIF could contribute to gain of surface GOM in  
440 non-urban area in most hours, which indicated higher GOM concentrations in the free  
441 troposphere. Figure 7 displays annual averaged diurnal profiles of the variation of  
442 HADV, VDIF, CHEM and AERO below 2 km. HADV played almost opposite roles in  
443 changing GOM concentration within the boundary layer in urban and non-urban areas  
444 (Figure 7a, b), but the trend of temporal variation and magnitude of contribution were  
445 about the same. It further indicated the transport of GOM from urban to non-urban  
446 areas which was the main source of GOM in upper air of non-urban areas. The  
447 contribution of VDIF to the GOM concentration is displayed in Figure 7c. More  
448 horizontally advected GOM aloft was mixed downwards to ground levels along with  
449 the increase of boundary layer height with the largest contribution of  $\sim 0.06 \text{ ng m}^{-3} \text{ h}^{-1}$   
450 at noon, which was why the contribution from VDIF was positive in the surface layer  
451 and negative in higher altitudes. CHEM was another contributor to the accumulation  
452 of GOM as well as AERO to PBM in the upper air, though CHEM and AERO seemed  
453 to be negligible to change GOM and PBM concentration in the surface layer. Figure  
454 7d-7f show that the contributions of CHEM and AERO were much higher in the upper  
455 layers than that at surface especially around noon since most of mercury chemical  
456 reactions rely on solar radiation. CHEM and AERO are the most important processes  
457 to transform GEM to GOM and PBM in the atmosphere. Within 2 km upon non-urban  
458 areas, the column concentration of GOM was increased by  $41.9 \text{ ng m}^{-2}$  owing to the  
459 transformation of GEM through CHEM and the column concentration of PBM was

460 enhanced by  $29.1 \text{ ng m}^{-2}$  through AERO in a whole day. The enhancements of GOM  
461 and PBM through CHEM and AERO in urban area was about 13% less than that in  
462 non-urban area. A combination of HADV, ZADV, VDIF, DDEP and CLDS tended to  
463 cancel out the gain of PBM from EMIS and AERO in urban area. In spite of most  
464 decrease from VDIF in urban area, the other four processes also make 21%  
465 contribution to remove surface PBM. However, both of HADV and ZADV  
466 transported PBM to surface layer in non-urban areas. The strongest increase of surface  
467 PBM occurred in the afternoon at 16-18 h due to higher emission rates of DOM and  
468 TRA which were the most important source for PBM while most of the decrease  
469 occurred in the morning between 9-11 h because the VDIF process was most effective  
470 then. In urban areas, the contribution from DDEP to PBM was 20% less than that  
471 from CLDS. In comparison, DDEP made 57% more contribution than CLDS to the  
472 loss of surface PBM in non-urban areas. The contribution from HDIF was negligible  
473 for all of GEM, GOM and PBM concentrations.

474

### 475 **3.3.2 Impacts of sources on processes**

476 Different mercury emission sources had different influences on processes due to  
477 the different distribution and intensity of emission sources. The contributions of  
478 natural sources and various anthropogenic sources to GEM processes in urban and  
479 non-urban areas of the YRD are compared in Figure 8. Various anthropogenic sources,  
480 especially CEM and PP, were the main sources leading to GEM advection out of  
481 urban areas with  $0.077 \text{ ng m}^{-3} \text{ h}^{-1}$  by HADV while natural sources mainly caused  
482 GEM to be horizontally transported away from non-urban areas with  $0.021 \text{ ng m}^{-3} \text{ h}^{-1}$   
483 (Figure 8a). ANTH made a similar contribution to DDEP and CHEM of GEM in both  
484 non-urban and urban areas. In comparison, natural sources affected DDEP and CHEM  
485 of GEM >110% more in non-urban than urban areas though emission from NAT in  
486 non-urban area only 38% more than that in urban area (Figure 8d, 8e). Conversely,

487 NAT caused comparable loss of GEM by VDIF in both areas and ANTH influenced  
488 VDIF of GEM in urban areas much more evidently (Figure 8c). In the YRD,  
489 emissions of GEM mostly came from CEM and PP which contributed locally to GEM  
490 concentrations with 0.32 and 0.27 ng m<sup>-3</sup> h<sup>-1</sup> in urban areas. More than 80% of the  
491 GEM emissions in non-urban areas were emitted by natural sources (Figure 8b).  
492 Totally, local emission in the YRD contributed 37.2% to the annual averaged GEM  
493 concentration in non-urban and 45.7% to that in urban areas.

494 Local emissions in the YRD were the primary source for GOM and PBM  
495 concentration with a contribution of 74.8% (92.9%) to GOM concentration and 44.0%  
496 (66.0%) to PBM concentration in non-urban (urban) area respectively. As GOM and  
497 PBM were the main constituents of mercury deposition, local emission in the YRD  
498 contributed 65.1% (88.7%) to the annual mercury dry deposition and 37.3% (56.2%)  
499 to mercury wet deposition in non-urban (urban) of YRD area. Obviously, local  
500 emissions have a larger influence on mercury concentration and deposition in urban  
501 areas. However, local emissions also were the most important factor for mercury  
502 pollution in non-urban areas. Figure 9 and Figure 10 show the contribution from  
503 different sources on the various processes of GOM and PBM in two areas. Natural  
504 sources only affected CHEM and AERO especially in non-urban areas significantly  
505 compared to anthropogenic sources (Figure 9e, 10e). IND was the largest contributor  
506 to all processes of GOM except for CHEM (Figure 9) while DOM contributed most to  
507 all processes of PBM besides of AERO (Figure 10). All anthropogenic sources  
508 increased the outflow of GOM and PBM from urban areas and enhanced the inflow  
509 into non-urban areas. Moreover, the quantity of inflow in non-urban areas was  
510 directly proportional to the outflow in urban areas which also indicates the influence  
511 of urban emissions on mercury pollution in non-urban areas via HADV (Figure 9a,  
512 10a). Figure 9c depicts that the effects of PP to VDIF of GOM were opposite to those  
513 of other anthropogenic sources. Emissions from PP enhanced the surface GOM

514 concentration by VDIF, which was because the emissions from PP was mostly in the  
515 free troposphere and formed a large concentration center there. Most of the GOM in  
516 higher altitudes would be diffused to the surface in local urban areas and others would  
517 be transported to non-urban areas and then increase surface GOM concentration there  
518 by VDIF. Due to the limited emissions of PBM from PP, the influence on VDIF of  
519 PBM from PP was negligible (Figure 10c).

520

#### 521 **4. Conclusion**

522 The simulation of atmospheric mercury in East China was conducted using  
523 CMAQ-Hg with a grid resolution in a nested domain of 27km to study source  
524 apportionment and process analysis. An updated mercury emission inventory for 2007  
525 with anthropogenic emission of 638 Mg year<sup>-1</sup> in China as well as emissions from  
526 natural sources of 551 Mg year<sup>-1</sup> was used for this simulation. The base model results  
527 were consistent with the measurements of atmospheric mercury including the  
528 concentration of TGM and PBM as well as the wet deposition in most sites of East  
529 China.

530 Model results for source apportionment showed that natural emissions are the  
531 most important source for GEM concentration in East China with a contribution of  
532 36.6%. However natural sources were less important in winter than anthropogenic  
533 sources due to significant seasonal variation of emissions. Among the anthropogenic  
534 sources, metal production (MET) and power plants (PP) were largest contributors to  
535 GEM. For GOM and PBM, anthropogenic sources dominated the variation of  
536 concentration with a contribution of 86.7% and 79.1% to the annual averaged  
537 concentrations. Industrial sources (IND) were responsible for 57.5% of the GOM  
538 concentration on average with the highest influence during winter time. IND also  
539 contributed significantly to PBM together with domestic sources (DOM) and they  
540 accounted for 58.8% of annual averaged PBM. 42.7% and 62.4% of wet and dry

541 deposition of mercury in East China came from anthropogenic sources respectively.  
542 Because of the large contribution to GOM and PBM, IND led to the most mercury  
543 deposition. Natural sources amounted a quarter of wet and dry deposition in summer  
544 owing to higher emissions and the increased photochemical oxidation to GOM and  
545 transformation to PBM during this season. The impact of mercury emitted from  
546 outside of China was also significant for mercury pollution in East China. This was  
547 indicated by a contribution of more than 30% from the model boundary conditions  
548 (BC) to GEM concentration and wet deposition.

549 The influence of atmospheric processes on mercury concentration in the near-  
550 surface layer was analyzed in urban and non-urban areas of the YRD. Emissions and  
551 vertical diffusion affected surface GEM and PBM concentration most and tended to  
552 compensate each other all the time in both urban and non-urban areas. However, dry  
553 deposition was the most important removal process for GOM with  $7.3 \text{ ng m}^{-3}$  and  $2.9$   
554  $\text{ng m}^{-3}$  deposited in urban and non-urban areas respectively on an average day. The  
555 variation of diurnal profiles of different processes (i.e.: HADV, VDIF, CHEM and  
556 AERO) inside the planetary boundary layer indicated the transport of mercury from  
557 urban to non-urban areas. Moreover, it was found that gas phase and aerosol  
558 chemistry (CHEM and AERO) have a large impact on GOM and PBM concentrations  
559 inside the free troposphere. The high concentration of GOM aloft in non-urban areas  
560 could be diffused downwards by VDIF. Most of anthropogenic sources caused  
561 mercury to be transported and diffused away from urban areas by HADV and VDIF  
562 and increased the concentration in non-urban areas by HADV. In contrast, emissions  
563 from power plants (PP) enhanced surface GOM concentration by VDIF because  
564 emission from PP led to a large concentration center in upper air. Natural sources only  
565 influenced CHEM and AERO in both areas more significantly than anthropogenic  
566 sources. Local emission in the YRD contributed 8.5% more to GEM and ~30% more  
567 to GOM and PBM in urban than those in non-urban areas.

568

569 **Acknowledgements**

570       This work was supported by the National Key Basic Research Development  
571 Program of China (2014CB441203,2011CB403406), the Specialized Research Fund  
572 for the Doctoral Program of Higher Education of China (20110091110010) and a  
573 project funded by the Priority Academic Program Development of Jiangsu Higher  
574 Education Institutions (PAPD). Thanks to Prof. Shuxiao Wang and Dr. Long Wang  
575 from Tsinghua University for providing mercury emission data.

576 **Reference**

- 577 Bieser, J., De Simone, F., Gencarelli, C., Geyer, B., Hedgecock, I., Matthias, V.,  
578 Travnikov, O. and Weigelt, A.: A diagnostic evaluation of modeled mercury wet  
579 depositions in Europe using atmospheric speciated high-resolution observations,  
580 *Environ. Sci. Pollut. Res.*, 21(16), 9995-10012, 2014.
- 581 Binkowski, F. S. and Roselle, S. J.: Models-3 Community Multiscale Air Quality  
582 (CMAQ) model aerosol component 1. Model description, *J. Geophys. Res.*, 108,  
583 4183–4201, doi:10.1029/2001JD001409, 2003.
- 584 Bullock, O. R. J. and Brehme, K. A.: Atmospheric mercury simulation using the  
585 CMAQ model: formulation description and analysis of wet deposition results,  
586 *Atmos. Environ.*, 36, 2135–2146, doi:10.1016/S1352-2310(02)00220-0, 2002.
- 587 Bullock, O. R., Atkinson, D., Braverman, T., Civerolo, K., Dastoor, A., Davignon, D.,  
588 Ku, J.-Y., Lohman, K., Myers, T. C., Park, R. J., Seigneur, C., Selin, N. E., Sistla,  
589 G., and Vijayaraghavan, K.: An analysis of simulated wet deposition of mercury  
590 from the North American Mercury Model Intercomparison Study, *J. Geophys.*  
591 *Res.*, 114, 1–12, doi:10.1029/2008JD011224, 2009.
- 592 Bullock, O. R., Atkinson, D., Braverman, T., Civerolo, K., Dastoor, A., Davignon, D.,  
593 Ku, J.-Y., Lohman, K., Myers, T. C., Park, R. J., Seigneur, C., Selin, N. E., Sistla,  
594 G., and Vijayaraghavan, K.: The North American Mercury Model  
595 Intercomparison Study (NAMMIS): Study description and model-to-model  
596 comparisons, *J. Geophys. Res.*, 113, 1–17, doi:10.1029/2008JD009803, 2008.
- 597 Chen, L., Liu, M., Xu, Z., Fan, R., Tao, J., Chen, D., Zhang, D., Xie, D. and Sun, J.:  
598 Variation Trends and Influencing Factors of Total Gaseous Mercury Inthe Pearl  
599 River Delta-A Highly Industrialised Region in South Chinainfluenced by  
600 Seasonal Monsoons. *Atmos. Environ.*, 77, 757-766, 2013.
- 601 Ci, Z.J., Zhang, X.S., Wang, Z.W. and Niu, Z.C.: Atmospheric gaseous elemental  
602 mercury (GEM) over a coastal/rural site downwind of East China: temporal

603 variation and long-range transport. *Atmos. Environ.*, 45, 2480-2487, 2011a.

604 Ci, Z.J., Zhang, X.S., Wang, Z.W., Niu, Z.C., Diao, X.Y. and Wang, S.W.: Distribution  
605 and air-sea exchange of mercury (Hg) in the Yellow Sea. *Atmos. Chem. Phys.* 11,  
606 2881-2892, 2011b.

607 Cohen, M., Artz, R., Draxler, R., Miller, P., Poissant, L., Niemi, D., Ratté, D.,  
608 Deslauriers, M., Duval, R., Laurin, R., Slotnick, J., Nettesheim, T., and  
609 McDonald, J.: Modeling the atmospheric transport and deposition of mercury to  
610 the Great Lakes, *Environ. Res.*, 95, 247-265, 2004.

611 Dou, H., Wang, S., Wang, L., Zhang, L. and Hao, J.: Characteristics of Total Gaseous  
612 Mercury Concentrations at a Rural Site of Yangtze Delta, China. *Environ. Sci.*  
613 (in Chinese), 34, 1-7, 2013.

614 Feng, X., Shang, L., Wang, S., Tang, S., and Zheng, W.: Temporal variation of total  
615 gaseous mercury in the air of Guiyang, China, *J. Geophys. Res.*, 109, D03303,  
616 doi:10.1029/2003JD004159, 2004.

617 Friedli, H.R., Arellano, A.F., Geng, and F., Pan, L.: Measurements of atmospheric  
618 mercury in Shanghai during September 2009, *Atmos. Chem. Phys.*, 11, 3781-  
619 3788, 2011.

620 Fu, X. W., Feng, X. B., Zhu, W. Z., Wang, S. F., and Lu, J.: Total gaseous mercury  
621 concentrations in ambient air in the eastern slope of Mt. Gongga, South-Eastern  
622 fringe of the Tibetan plateau. *China. Atmos. Environ.* 42, 970–979, 2008

623 Gbor, P. K., Wen, D., Meng, F., Yang, F., Zhang, B. and Sloan, J. J.: Improved model  
624 for mercury emission, transport and deposition, *Atmos. Environ.* 40, 973-983,  
625 2006.

626 Gbor, P., Wen, D., Meng, F., Yang, F., and Sloan, J.: Modeling of mercury emission,  
627 transport and deposition in North America, *Atmos. Environ.*, 41, 1135–1149,  
628 doi:10.1016/j.atmosenv.2006.10.005, 2007.

629 Holloway, T., Viogt, C., Morton, J., Spak, S. N., Rutter, A. P. and Schauer, J. J.: An



630 assessment of atmospheric mercury in the Community Multiscale Air Quality  
631 (CMAQ) model at an urban site and a rural site in the Great Lakes Region of  
632 North America, *Atmos. Chem. Phys.*, 12, 7117-7133, 2012.

633 Keeler, G. J., Gratz, L. E., and Al-Wali, K.: Long-term Atmospheric Mercury Wet  
634 Deposition at Underhill, Vermont, *Ecotoxicology*, 14, 71–83, 2005.

635 Lin, C. J. and Pehkonen, S. O.: The chemistry of atmospheric mercury: A review,  
636 *Atmos. Environ.*, 33, 2067–2079, 1999.

637 Lin, C. J., Pan, L., Steets, D. G., Shetty, S. K., Jang, C., Feng, X., Chu, H. W. and Ho,  
638 T. C.: Estimating mercury emission outflow from East Asia using CMAQ-Hg,  
639 *Atmos. Chem. Phys.*, 10, 1853-1864, 2010.

640 Lin, C. J., Shetty, S. K., Pan, L., Pongprueksa, P., Jang, C. and Chu, H.: Source  
641 attribution for mercury deposition in the contiguous United States: Regional  
642 difference and seasonal variation, *J. Air Waste Manage*, 62(1), 52-63, 2012.

643 Lin, X. and Tao, Y.: A numerical modelling study on regional mercury budget for  
644 eastern North America, *Atmos. Chem. Phys.*, 3, 535-548, 2003.

645 Lindberg, S. E., Brooks, S., Lin, C. J., Scott, K. J., Landis, M. S., Stevens, R. K.,  
646 Goodsite, M., and Richter, A.: Dynamic oxidation of gaseous mercury in the  
647 arctic troposphere at polar sunrise, *Environ. Sci. Technol.*, 36, 1245–1256,  
648 doi:10.1021/es0111941, 2002.

649 Liu, X. and Zhang, Y: Understanding of the formation mechanisms of ozone and  
650 particulate matter at a fine scale over the southeastern U.S.: Process analyses and  
651 responses to future-year emissions, *Atmos. Environ.*, 74, 259-276, 2013.

652 Nguyen, D., Kim, J., Shim, S. and Zhang, X.: Ground and shipboard measurements of  
653 atmospheric gaseous elemental mercury over the Yellow Sea region during  
654 2007–2008, *Atmos. Environ.*, 41, 253-260, 2011.

655 Pacyna, E.G., Pacyna, J.M., Sundseth, K., Munthe, J., Kindbom, K., Wilson, S.,  
656 Steenhuisen, F., and Maxson, P.: Global emission of mercury to the atmosphere

657 from anthropogenic sources in 2005 and projections to 2020. *Atmospheric*  
658 *Environment* 44, 2487-2499, 2010.

659 Pai, P., Karamchandani, P., Seigneur, C. and Allan M.: Sensitivity of simulated  
660 atmospheric mercury concentrations and deposition to model input parameters, *J.*  
661 *Geophys. Res.*, 104, 13855-13868, 1999.

662 Pan, L., Lin, C. J., Carmichael, G. R., Streets, D. G., Tang, Y., Woo, J. H., Shetty, S.  
663 K., Chu, H. W., Ho, T. C., Friedli, H. R. and Feng, X.: Study of atmospheric  
664 mercury budget in East Asia using STEM-Hg modeling system, *Sci. Total*  
665 *Environ.*, 408, 3277-3291, 2010.

666 Pongprueksa, P., Lin, C. J., Lindberg, S.E., Jang, C., Braverman, T., Russell Bullock  
667 Jr., O., Ho, T. C. and Chu, H. W.: Scientific uncertainties in atmospheric mercury  
668 models III: boundary and initial conditions, model grid resolution, and Hg(II)  
669 reduction mechanism. *Atmos. Environ.*, 42(8), 1828–1845, 2008.

670 Quan, J., Zhang, Q. and Zhang, X.: Emission of Hg from coal consumption in China  
671 and its summertime deposition calculated by CMAQ-Hg, *Terr. Atmos. Ocean.*  
672 *Sci.*, 20,325-331, 2009.

673 Rolfhus, K.R., Sakamoto, H.E., Cleckner, L.B., Stoor, R.W., Babiarz, C.L., Back,  
674 R.C., Manolopoulos, H., Hurley, J.P.: Distribution and fluxes of total and methyl  
675 mercury in Lake Superior. *Environ. Sci. and Technol.*, 37, 865–872, 2003.

676 Sarwar, G., Luecken, D., Yarwood, G., Whitten, G. Z., and Carter, W. P. L.: Impact of  
677 an Updated Carbon Bond Mechanism on Predictions from the CMAQ Modeling  
678 System: Preliminary Assessment, *J. Appl. Meteorol. Clim.*, 47, 3–14,  
679 doi:10.1175/2007JAMC1393.1, 2008.

680 Schroeder, W.H., and Munthe, J.: Atmospheric mercury—an overview. *Atmos.*  
681 *Environ.* 32, 809–822, 1998.

682 Seigneur, C., Vijayaraghavan, K., Lohman, K., Karamchandani, P., and Scott, C.:  
683 Global Source Attribution for Mercury Deposition in the United States, *Environ.*

684 Sci. Technol., 38, 555-569, 2004.

685 Selin, N. E., and Jacob, D. J.: Seasonal and spatial patterns of mercury wet deposition  
686 in the United States: constraints on the contribution from North American  
687 anthropogenic sources, *Atmos. Environ.*, 42 (21), 5193–5204, 2008.

688 Selin, N. E., Jacob, D. J., Park, R. J., Yantosca, R. M., Strode, S., Jaegle, L., and Jaffe,  
689 D.: Chemical cycling and deposition of atmospheric mercury: Global constraints  
690 from observations, *J. Geophys. Res.-Atmos.*, 112, D02308,  
691 doi:10.1029/2006jd007450, 2007.

692 Shetty, S., Lin, C., Streets, D., and Jang, C.: Model estimate of mercury emission  
693 from natural sources in East Asia, 42, 8674-8685, 2008.

694 Streets, D. G., Zhang, Q. and Wu, Y.: Projections of global mercury emissions in  
695 2050, *Environ. Sci. Technol.*, 36(8), 2983-2988, 2009.

696 Wan, Q., Feng, X.B., Lu, J.L., Zheng, W., Song, X.J., Li, P., Han, S.J., and Xu, H.:  
697 Atmospheric mercury in Changbai Mountain area, northeastern China I: the  
698 season distribution pattern of total gaseous mercury and its potential sources.  
699 *Environ. Res.* 109, 201–206, 2009.

700 Wang, L., Wang, S., Zhang, L., Wang, Y., Zhang, Y., Nielsen, C., McElroy, M. B. and  
701 Hao, J.: Source apportionment of atmospheric mercury pollution in China using  
702 the GEOS-Chem model, *Environ. Pollut.*, 190, 166-175, 2014.

703 Wang, Y.: The speciation, levels and potential impacted factors of atmospheric  
704 mercury in Hefei, Central China (in Chinese), University of Science and  
705 Technology of China, 2010.

706 Wang, S.X., Zhang, L., Wang, L., Wu, Q.R., Wang, F. Y. and Hao, J. M.: A review of  
707 atmospheric mercury emissions, pollution and control in China. *Front. Environ.*  
708 *Sci. Eng.*, DOI: 10.1007/s11783-014-0673-x, 2014.

709 Wang, Z.W., Chen, Z.S., Duan, N., and Zhang, X.S.: Gaseous elemental mercury  
710 concentration in atmosphere at urban and remote sites in China. *J. Environ. Sci.*

711 19, 176–180, 2007.

712 Wu, Q.R., Wang, S.X., Zhang, L., Song, J.X., Yang, H. and Meng, Y.: Update of  
713 mercury emissions from China's primary zinc, lead and copper smelters, 2000-  
714 2010, *Atmos. Chem. Phys.*, 12, 11153-11163, 2012.

715 Wu, Y., Wang, S., Streets, D. G., Hao, J., Chan, M. and Jiang, J.: Trends in  
716 Anthropogenic Mercury Emissions in China from 1995 to 2003. *Environ. Sci.*  
717 *Technol.*, 40, 5312-5318, 2006.

718 Xiu, G., Cail, J., Zhang, W., Zhang, D., Bueler, A., Lee, S., Shen, Y., Xu, L., Hunag,  
719 X., Zhang, P.: Speciated mercury in size-fractionated particles in Shanghai  
720 ambient air. *Atmos. Environ.*, 43, 3145-3154, 2009.

721 Zhang, L., Wang, S. X., Wang, L. and Hao, J. M.: Atmospheric mercury concentration  
722 and chemical speciation at a rural site in Beijing, China: implications of mercury  
723 emission sources. *Atmos. Chem. Phys.*, 13, 10505–10516, 2013.

724 Zhu, J., Wang, T., Talbot, R., Mao, H., Hall, C. B., Yang, X., Fu, C., Zhuang, B., Li,  
725 S., Han, Y. and Huang, X.: Characteristics of atmospheric Total Gaseous  
726 Mercury (TGM) observed in urban Nanjing, China. *Atmos. Chem. Phys.*, 12,  
727 12103–12118, 2012.

728 Zhu, J., Wang, T., Talbot, R., Mao, H., Yang, X., Fu, C., Sun, J, Zhuang, B., Li, S.,  
729 Han, Y. and Xie, M.: Characteristics of atmospheric mercury deposition and size-  
730 fractionated particulate mercury in urban Nanjing, China. *Atmos. Chem. Phys.*,  
731 12, 2233–2244, 2014.

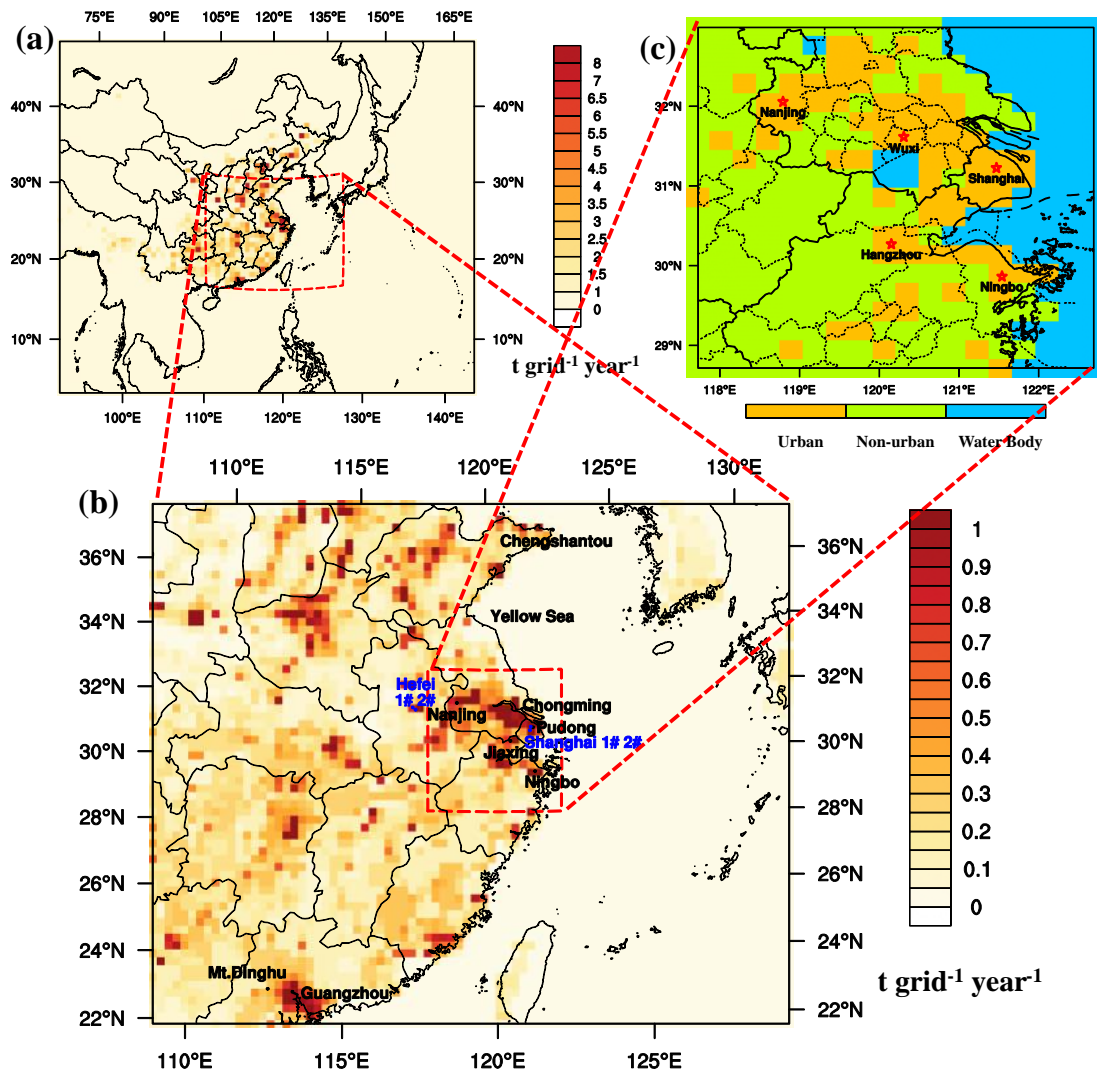
732

733

Table 1 Summary of mercury emissions in the model domain 1

	<b>GEM(Mg/year)</b>	<b>GOM(Mg/year)</b>	<b>TPM(Mg/year)</b>	<b>Total(Mg/year)</b>
<b>Natural</b>	551	0	0	551
<b>Anthropogenic</b>	316	245	77	638
<b>CEM</b>	69.0	12.9	4.3	86.2
<b>DOM</b>	6.4	9.2	24.7	40.3
<b>IND</b>	34.1	149.0	27.2	210.3
<b>MET</b>	100.6	30.1	5.3	136.0
<b>PP</b>	84.2	38.1	1.3	123.6
<b>TRA</b>	8.1	5.9	14.0	28.0
<b>Total</b>	867	245	77	1189

734



735

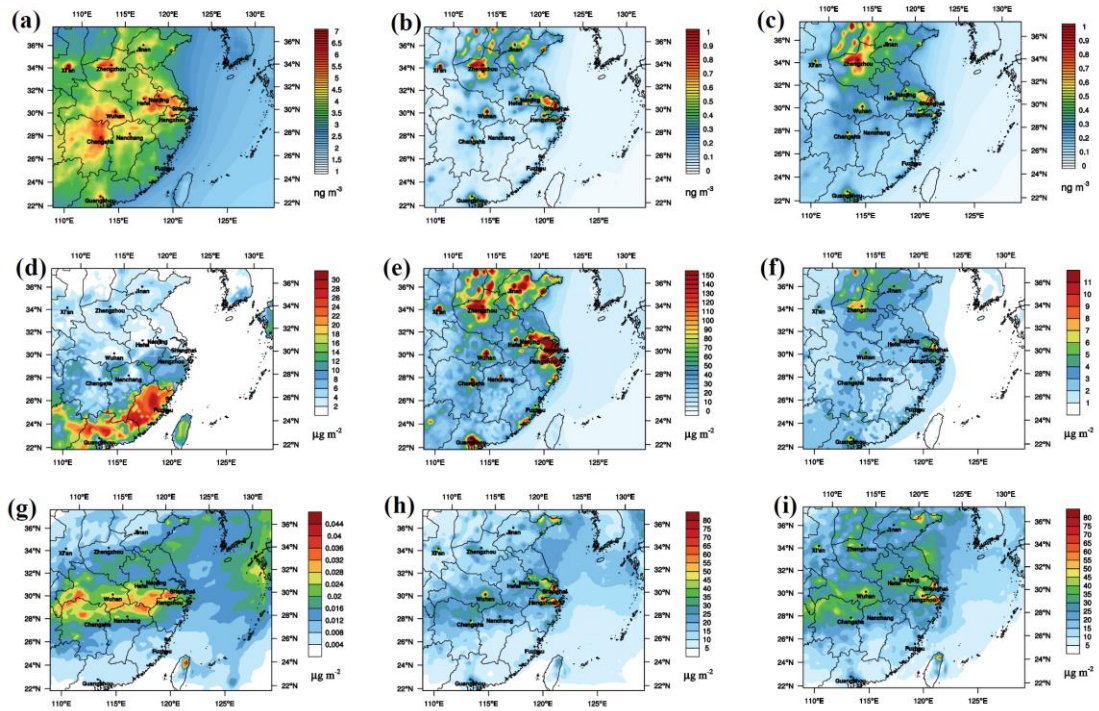
736 Figure 1 Model domain (a) Domain 1 with annual total mercury emission (b) Domain

737 2 with annual total mercury emission (c) Yangtze River Delta (YRD) area with land

738

use category

739



740

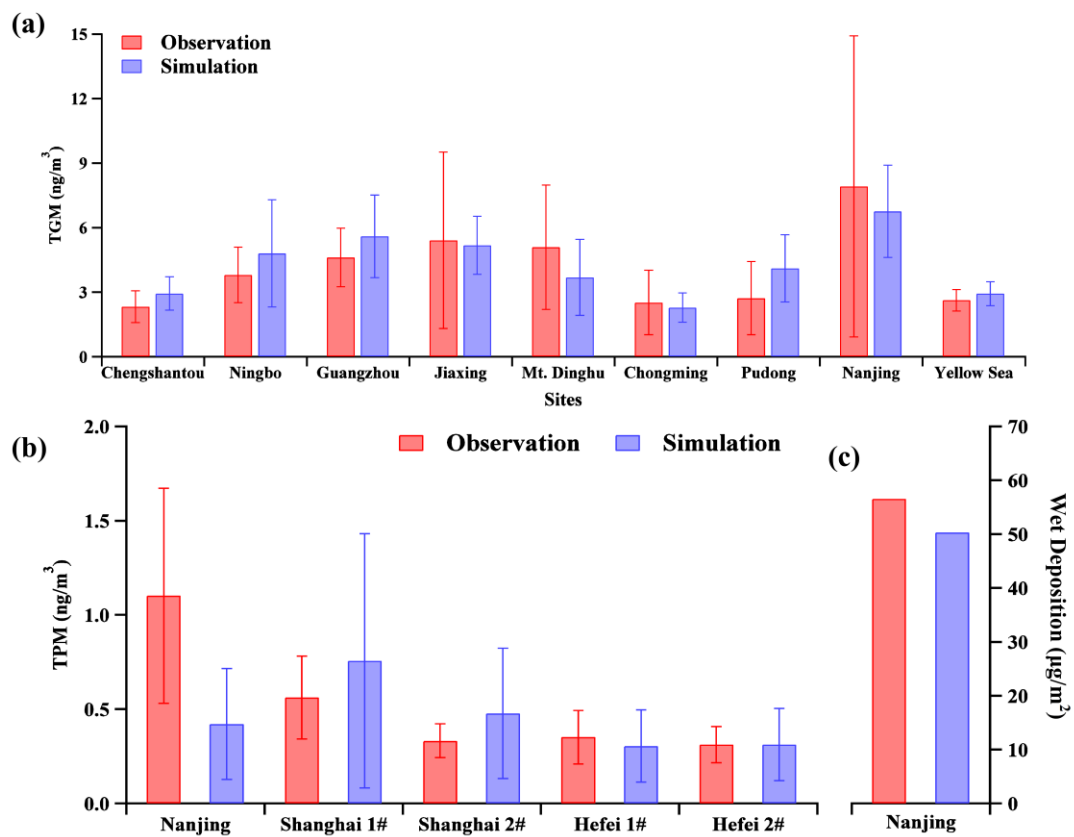
741 Figure 2 Simulated annual average concentration of (a) GEM, (b) GOM and (c) PBM,

742 annual dry deposition of (d) GEM, (e) GOM and (f) PBM and dry deposition of (g)

743

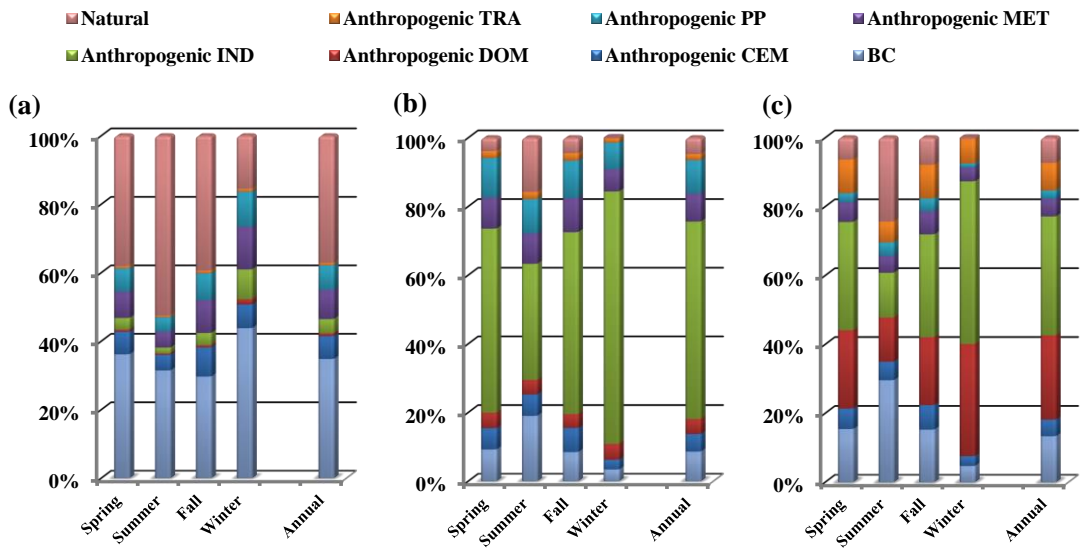
GEM, (h) GOM and (i) PBM in East China in 2011

744



745  
746 Figure 3 Comparison between simulated results and measurements in sites for (a)  
747 TGM concentration, (b) PBM concentration and (c) wet deposition.  
748



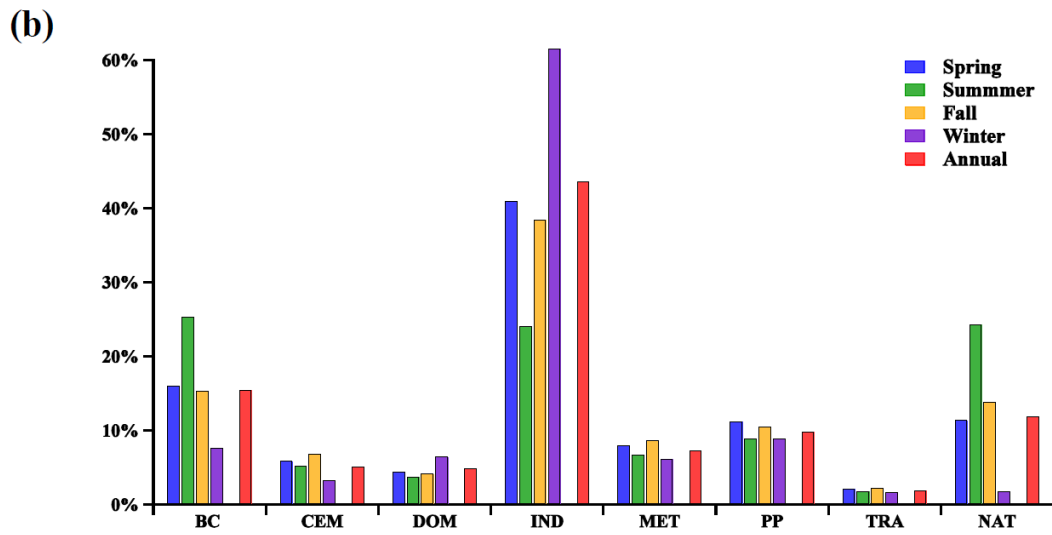
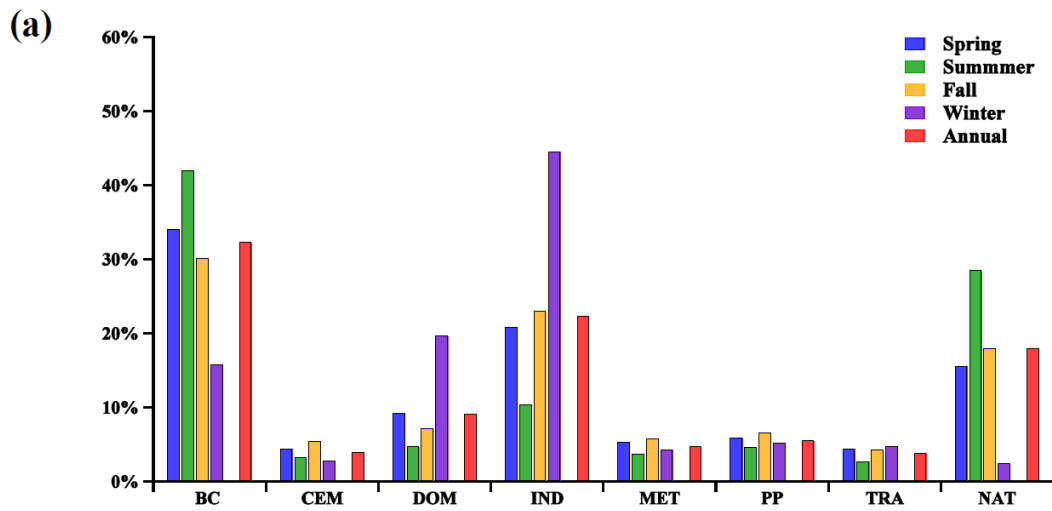


749

750 Figure 4 Source contributions to seasonal and annual averaged (a) GEM (b) GOM (c)

751

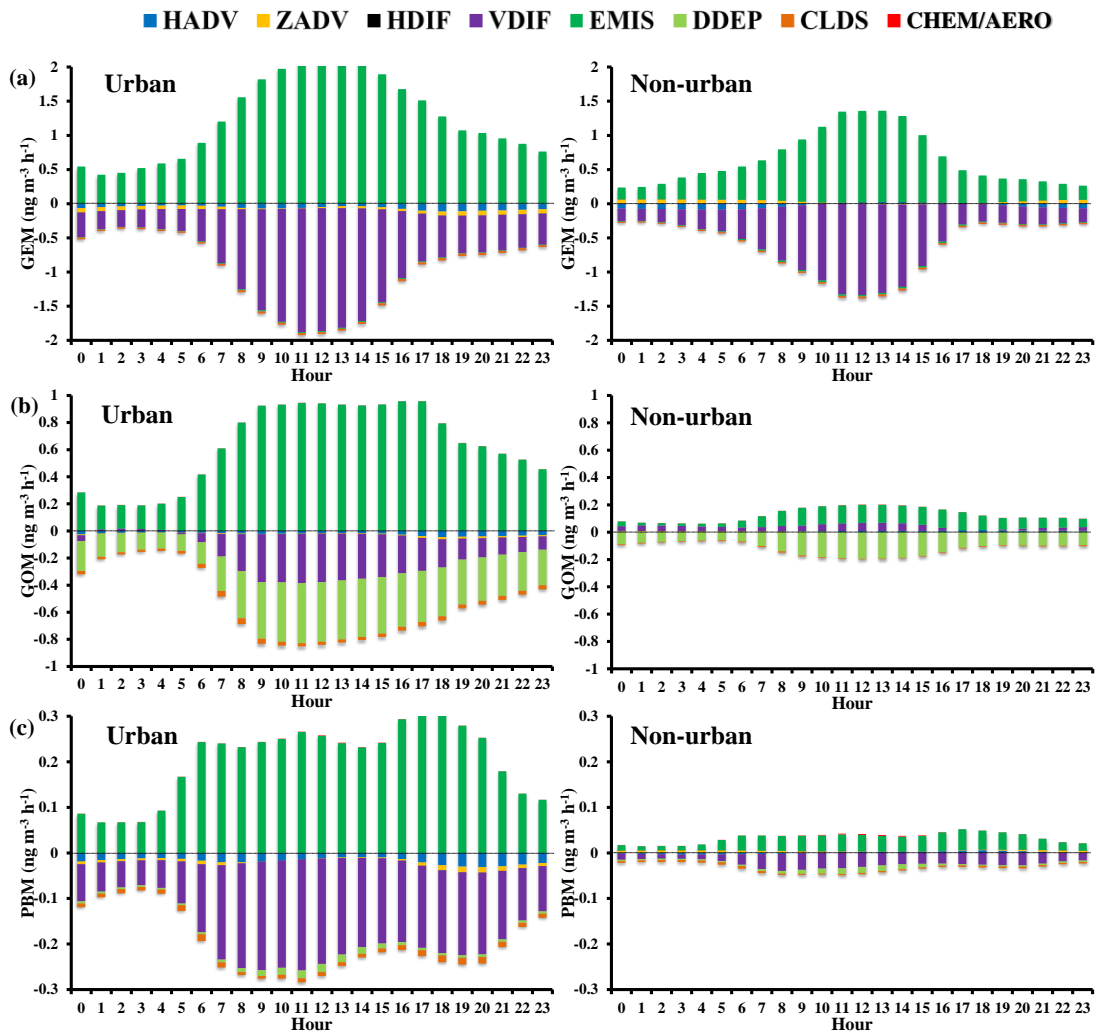
PBM concentration.



752

753 Figure 5 Source contributions to seasonal and annual mercury (a) wet and (b) dry  
 754 deposition

755



756

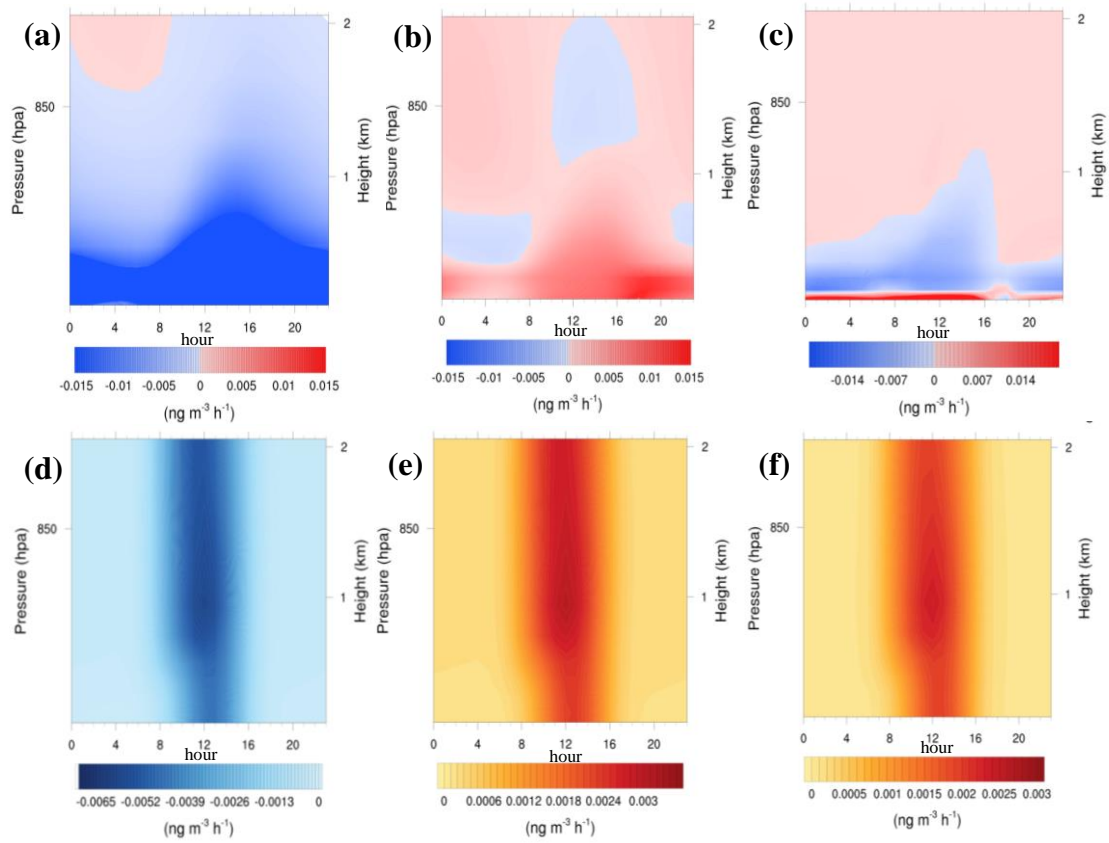
757 Figure 6 Diurnal variations of processes of (a) GEM, (b) GOM and (c) PBM in urban

758

and non-urban area.

759

760



761

762

Figure 7 Profile of the contribution of (a) HADV to GOM in urban area and (b)

763

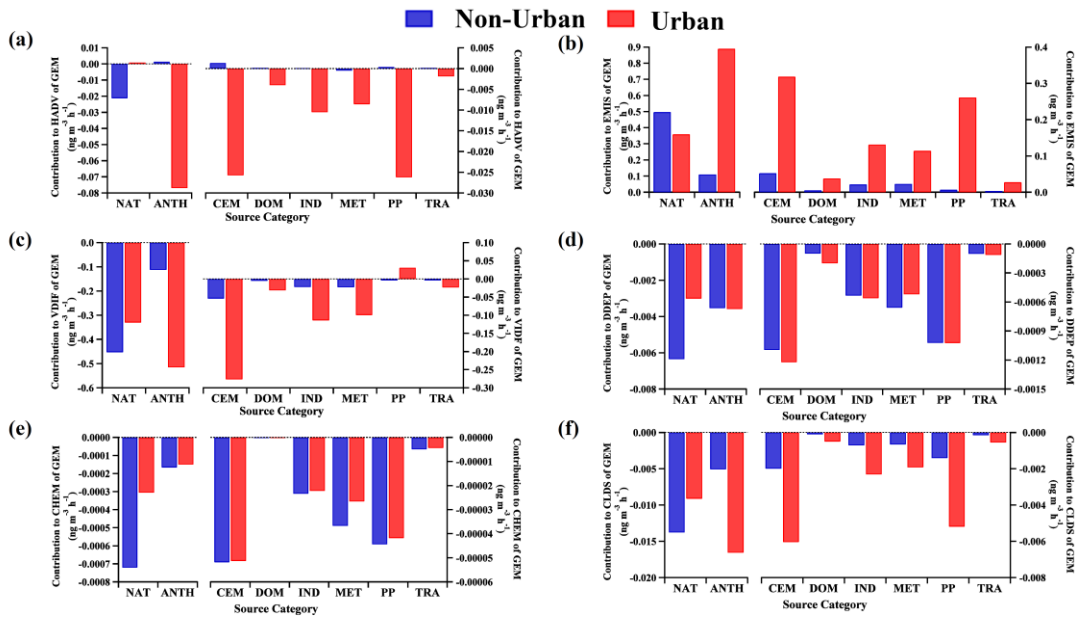
HADV to GOM, (c) VDIF to GOM, (d) CHEM to GEM, (e) CHEM to GOM, (f)

764

AERO to PBM in non-urban area.

765

766



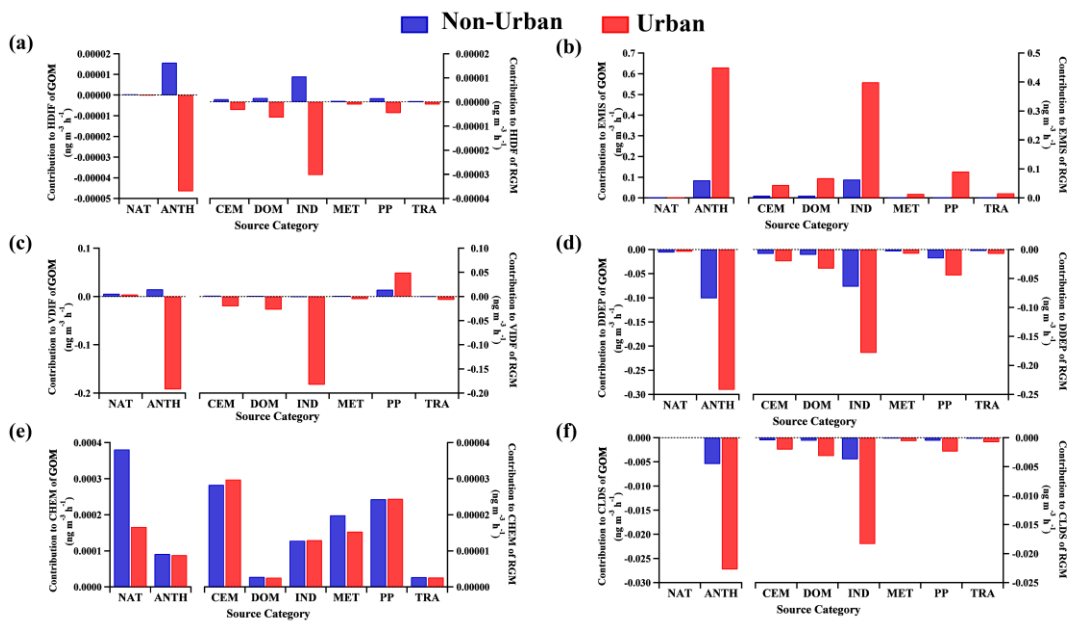
767

768 Figure 8 Impact of emission sources on (a) HADV, (b) EMIS, (c) VDIF, (d) DDEP, (e)

769

CHEM and (f) CLDS processes of GEM

770

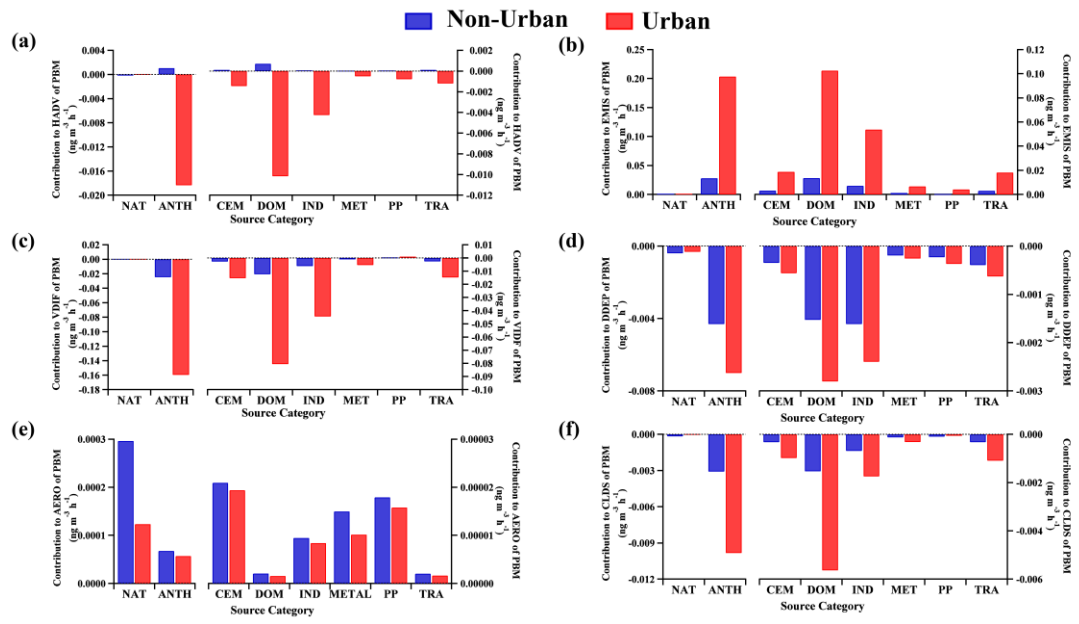


771

772 Figure 9 Impact of emission sources on (a) HADV, (b) EMIS, (c) VDIF, (d) DDEP, (e)

773

CHEM and (f) CLDS processes of GOM



774

775 Figure 10 Impact of emission sources on (a) HADV, (b) EMIS, (c) VDIF, (d) DDEP,

776

(e) AERO and (f) CLDS processes of PBM